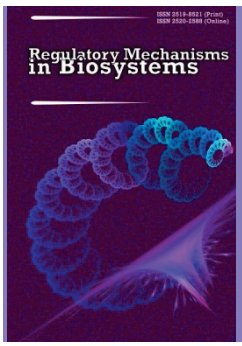

Regulatory Mechanisms in Biosystems

ISSN 2519-8521 (Print)
ISSN 2520-2588 (Online)
Regul. Mech. Biosyst.,
2022, 13(3), 272–280
doi: 10.15421/022235

The whole-cell kinetic metabolic model of the pH regulation mechanisms in human erythrocytes

O. I. Dotsenko

Vasyl' Stus Donetsk National University, Vinnytsia, Ukraine

Article info

Received 30.05.2022
Received in revised form 26.06.2022
Accepted 27.06.2022

Vasyl' Stus Donetsk National University, 600-richya st., 21, Vinnytsia 21021, Ukraine.
Tel.: +38-093-724-66-10.
E-mail: dots_don@ukr.net

Dotsenko, O. I. (2022). The whole-cell kinetic metabolic model of the pH regulation mechanisms in human erythrocytes. Regulatory Mechanisms in Biosystems, 13(3), 272–280. doi:10.15421/022235

Mathematical modeling in recent years helped to obtain answers to questions that were difficult or even impossible to answer experimentally, to predict several unexpected connections in cell metabolism and to understand and importance of certain biochemical reactions. Due to the complexity and variety of processes underlying the mechanisms of intracellular pH (pHi) regulation, mathematical modeling and metabolome analysis are powerful tools for their analysis. In this regard, a mathematical metabolic model for human erythrocytes was created, which combines cellular metabolism with acid-base processes and gas exchange. The model consists of the main metabolic pathways, such as glycolysis, the pentose phosphate pathway, some membrane transport systems, and interactions between hemoglobin and metabolites. The Jacobs-Stewart cycle, which is fundamental in gas exchange and pH regulation, was included to these pathways. The model was created in the COPASI environment, consisted of 85 reactions, the rate of which is based on accurate kinetic equations. The time dependences of reaction flows and metabolite concentrations, as an outcome of calculations, allowed us to reproduce the behaviour of the metabolic system after its disturbance in vitro and to establish the recovery mechanisms or approximation to stationary states. The COPASI simulation environment provides model flexibility by reproducing any experimental design by optimizing direct quantitative comparisons between measured and predicted results. Thus, the procedure of parameters optimization (Parameter Estimation) followed by the solution of the model's differential equations (Time Course procedure) was used to predict the behaviour of all measured and unmeasured variables over time. The initial intracellular concentrations of CO_2, HCO_3^- in human erythrocytes used for incubation in a phosphate buffer medium were calculated. Changes in CO_2, HCO_3^- content over time were shown. It was established that the regulation of pH in erythrocytes placed in a buffer medium takes place with the participation of two types of processes – fast (takes place in 1.3 s) and slow. It is shown that fast processes are aimed at restoring the intracellular balance between CO_2 and HCO_3^-, slow processes are aimed at establishing the balance of H^+ between the cell and the extracellular environment. The role of carbonic anhydrase (CA) and hemoglobin in the processes of pH stabilization is shown and analyzed. The physiological role of the metabolon between band 3 protein (AE1), CA, aquaporin and hemoglobin in maintaining pH homeostasis in the conditions of *in vitro* experiments are discussed.

Keywords: carbonic anhydrase; anion exchanger AE1; gas exchange; Jacobs-Stewart cycle; bicarbonate; COPASI.

Introduction

Monitoring intracellular pH has importance in understanding intracellular metabolism and functions (Chao et al., 2018; Michl et al., 2019; Huang et al., 2020; Doyen et al., 2022). Protein-protein, protein-ligand, protein-membrane interactions are highly dependent on the pH value, so pH is an important factor affecting the functioning of macromolecules and a whole-cell. At the cellular level, maintenance of cytosolic pH (intracellular pH, pHi) within a narrow range is important for many processes, including biochemical reactions, functions of transporters, channels, receptors, structural proteins, and regulatory molecules (Boron, 2010; Occhipinti & Boron, 2015; Shartau et al., 2016; Calvetti et al., 2020). The pH gradients determine the direction and time of macromolecular interactions. In this context, several molecular mechanisms evolved for solving the problem of pH regulation by transporting acid-base equivalents across membranes (Hsu, 2018; Lee & Hong, 2020; Li et al., 2021; Michenkova et al., 2021; Doyen et al., 2022).

Erythrocytes are special cells because they carry out the transport of HCO_3^- ions to enhance the transfer of CO_2 from the systemic circulation capillaries to the pulmonary capillaries (Boron, 2010; Jennings, 2021). These cells play a fundamental role in regulating the acid-base balance of extracellular fluids. The same CO_2/HCO_3^- buffer pair is involved in regulating intracellular pH. The key molecular elements involved in pHi stabilization in erythrocytes are hemoglobin (Hb), isoform of anion exchange transporter AE1 (band 3 protein), the enzyme carbonyl anhydrase (CA) and aquaporin (AQP1). Hemoglobin at a concentration of 7 mM per liter of cellular water ($mM \cdot (L \text{ of cellular water})^{-1}$) is the main proton buffer of erythrocytes (Swietach et al., 2010). AE1, expressed in more than 10^6 copies per human erythrocyte (Swietach et al., 2010; Johnson & Casey, 2011; Bertocchio et al., 2020; Jennings, 2021; Kalli & Reithmeier, 2022), mediates the rapid transmembrane exchange of Cl^- to HCO_3^-, thereby increasing the mass transport of CO_2 in the form of HCO_3^- in the blood plasma (Lee & Hong, 2020; Lüscher et al., 2020).

AE1 activity is facilitated by cytoplasmic carbonic anhydrase (CA), which catalyzes the reversible hydration of carbon dioxide (Geers & Gros, 2000; Rasmussen & Boedtkjer, 2018). The water required for this reaction is supplied by AQP1 (Hsu, 2018; Michenkova et al., 2021). Any process that leads to a local change of H^+, CO_2, HCO_3^- disrupts the steady-state level of intracellular pH (Swietach et al., 2010; Occhipinti & Boron, 2015; Occhipinti & Boron, 2019). The loss of the ability to restore the stationary pH level during storage of erythrocytes also affects the affinity of hemoglobin for oxygen transfer, therefore, disrupts the functional properties of cells (Zimna et al., 2021). To study metabolic processes in erythrocytes, *in vitro* experiments are widely used, including washing cells, their incuba-

tion in buffer solutions of various compositions. These procedures change the intracellular pH (Meryman & Hornblower, 1991) and consequently the activity of cellular reactions that are pH dependent. However, few people pay attention to this in such studies. In this connection, difficulties arise with the reproducibility of the results and their interpretation. The transmembrane flux of any substance could affect the transmembrane gradients of all others, creating complex interdependencies that cannot be understood by intuition alone. And although the role of erythrocytes in the regulation of plasma pH has been widely studied (Swietach et al., 2010), much less is known about the dynamics of hydrogen ions inside the erythrocytes themselves.

The dynamics of pH cannot simply be described as a combination of transporter rates and enzyme activities because their activities are linked to other metabolic reactions, even if they do not directly affect pH. Furthermore, since protonation reactions are numerous within the cell, it is also imperative that cellular chemistry is fully considered as it affects the availability of substrates for transporters and the protonation and deprotonation of groups that act as buffers (Doyen et al., 2022). Even at the level of a single cell, perturbations in acid-base reactions, diffusion and transport are so complex that they cannot be understood without a quantitative model (Boron, 2010; Occhipinti & Boron, 2015).

Due to the complexity and diversity of the processes underlying pHi regulation, mathematical modeling and metabolome analysis are powerful tools for analyzing complex, dynamic, and large-scale systems (Occhipinti & Boron, 2015, Occhipinti & Boron, 2019; Doyen et al., 2022). The construction of mathematical and computational models can provide valuable information about the mechanisms of intracellular regulation, pH in particular. This prompts researchers to develop mathematical models of acid-base hemostasis (Geers & Gros, 2000; Rees et al., 2010; Al-Samir et al., 2013; O'Neill & Robbins, 2017, Cherif et al., 2020; Doyen et al., 2022). Mathematical models of blood acid-base chemistry, based on the equations of the laws of active masses and mass balance, have found application as diagnostic tools in intensive care (Cherif et al., 2020; Leypoldt et al., 2020). However, some of them are focused on the study of gas exchange between erythrocytes and blood plasma, others include a small number of reactions involved in the Jacobs-Stewart cycle and do not consider the relationships with other reactions that may affect them. Some models are difficult to apply to the analysis of experimental data.

As computational methods improve, it becomes possible to model the functioning and relationships of many metabolic reactions. The combination of computational approaches and a huge stock of existing (and future) experimental data has the potential to reach a true understanding of the molecular mechanisms (Nishino et al., 2013; Dotsenko, 2016; Jennings, 2021) of processes, as well as the principles of their regulation by various physical or chemical factors, including pH and temperature.

Thus, the goal of the work was to create a mathematical metabolic model of erythrocytes, which combines cellular metabolism with acid-base processes and gas exchange. The model provides the ability to quantify the current value of intracellular pH, based on a small set of experimental data, such as the composition of the extracellular medium and the initial value of intracellular pH. So far, the model has been used to analyze the mechanisms of pH regulation in human erythrocytes *in vitro*. Along with this, the model allows one: a) to predict the course of processes and the content of metabolites in the cell depending on the value of intracellular pH in *in vitro* experiments, b) to analyze experimental data more accurately and qualitatively, c) to save time and money by performing a smaller number of experimental studies.

Materials and methods

Mathematical model and modeling methods. Model creation and all numerical calculations based on the mathematical model of human erythrocyte metabolism were carried out using the simulation environment COPASI 4.36. The model includes two compartments, 85 reactions and 99 metabolites. The reactions included in the model are shown in Table 1, the metabolic scheme reproduced in the model is shown in Figure 1. The model is based on exact kinetic equations.

The published model of human erythrocyte metabolism from BioModels Database (www.ebi.ac.uk/biomodels/MODEL5950552398#Files) was used as the basic model (Mulquiney & Kuchel, 1999). The basic model consists of the main metabolic pathways of human erythrocytes (53 reactions), such as glycolysis, the pentose phosphate pathway, some membrane transport systems of intermediate products, reactions of the interaction between hemoglobin and metabolites. In this model, certain enzymatic reactions of glycolysis are controlled by the enzymes hexokinase (HK), phosphofructokinase (PFK), glyceraldehyde phosphate dehydrogenase (GAPDH), pyruvate kinase (PK), lactate dehydrogenase (LDH), 2,3-diphosphoglycerate (2,3-DPG) shunt reactions are presented as pH-dependent kinetics. In addition, we added the reactions of the interaction of band 3 protein with ligand forms of Hb and glycolytic enzymes, such as PFK, aldolase (ALD), GAPDH and LDG. The kinetics of these interactions are described Nishino et al. (2013). The effects of inorganic phosphates and adenine nucleotides, which can serve as allosteric effectors of glycolysis, were included in the model, as in recent mathematical models of erythrocytes (Kinoshita, 2007; Nishino et al., 2013).

The created model includes two compartments: intracellular and extracellular, which allows one to study the influence of the composition of the external environment (primarily the content of gases) on the processes taking place in the cell. The extracellular space was treated as a well-mixed compartment of infinite size, and the unmixed layers around the cells were not considered.

The transition of hemoglobin between oxygenated (R-) and deoxygenated states (T-state) depending on pH, temperature and 2,3-BPG level is described as in (Nishino et al., 2013) using the following ratios:

$$S_{HbO_2} = \frac{[HbO_2]}{[Hb]} = \frac{K_{HbO_2} \cdot [O_2]^n}{1 + K_{HbO_2} \cdot [O_2]^n},$$

where S_{HbO_2} – the degree of saturation of hemoglobin with oxygen.

$$K_{HbO_2} = \frac{K_4^{'}\left(K_3^{'}[CO_2]\left(1 + \frac{K_3^{"}}{10^{-pHi}}\right) + \left(1 + \frac{10^{-pHi}}{K_6^{"}}\right)\right)}{\left(K_2^{'}[CO_2]\left(1 + \frac{K_2^{"}}{10^{-pHi}}\right) + \left(1 + \frac{10^{-pHi}}{K_5^{"}}\right)\right)},$$

$$K_4^{'} = K_4^{"}\left(\frac{(10^{-pHi})_s}{10^{-pHi}}\right)^{n1}\left(\frac{[CO_2]_s}{[CO_2]_{out}}\right)^{n2}\left(\frac{[2,3-BPG]_s}{[2,3-BPG]}\right)^{n3}\left(\frac{T_s}{T}\right)^{n4},$$

$$[O_2]_{out} = \frac{10^{-6}\left(1,37 - 0,0137(T-37) + 0,00058(T-37)^2\right)\cdot 0,65 \cdot P_{O_2 out}}{0,94},$$

$$[CO_2]_{out} = \frac{10^{-5}\left(3,07 - 0,057(T-37) + 0,002(T-37)^2\right)\cdot 0,65 \cdot P_{CO_2 out}}{0,94}.$$

$$n1 = -6,775 + 2,0372 \cdot pHi - 0,1235 \cdot pHi^2,$$

$$n2 = -0,008765 + 0,00086 \cdot P_{CO_2 out} + 6,3 \cdot 10^{-7} \cdot P^2_{CO_2\,out},$$

$$n3 = 0,2583 + 28,6978 \cdot [2,3-BPG] - 917,69 \cdot [2,3-BPG]^2,$$

$$n4 = 1,6914 + 0,0618 \cdot T + 0,00048 \cdot T^2.$$

$$pHi = -\lg[H^+]_{in},$$

$$K_2^{'} = 2.4 \cdot 10^{-5}, K_2^{"} = 1 \cdot 10^{-6}, K_3^{'} = 2.4 \cdot 10^{-5}, K_3^{"} = 5.0 \cdot 10^{-5},$$

$$K_4^{"} = 6.77 \cdot 10^{11}, K_5^{"} = 7.2 \cdot 10^{-8}, K_6^{"} = 8.4 \cdot 10^{-9}, n = 2,7,\ T = 25^0 C, P_{O_2} = 159\,mmHg, P_{CO_2} = 3.04\,mmHg,$$

$[CO_2]_s$, pH_s, T_s – values typical for erythrocytes: 1.23 mM (Geers & Gros, 2000), 7.24, 37 °C, respectively, $[2,3-BPG]_s = 4.65\,mM$ (Nishino et al., 2013).

Development of the pH homeostasis cycle. Carbon dioxide. The content of intracellular CO_2 consists of the formation or consumption of CO_2 via a) intracellular and extracellular hydration-dehydration reactions, b) CO_2 exchange with the incubation medium, and c) the reaction of CO_2 with hemoglobin.

a) hydration-dehydration of CO_2 occurs according to the reaction:

$$CO_2 + H_2O \underset{kv}{\overset{ku}{\rightleftarrows}} H_2CO_3 \overset{K}{\rightleftarrows} H^+ + HCO_3^-.$$

It was believed that in the extracellular environment, CO_2 hydrates non-enzymatically, and inside cells it metabolizes by carbonic anhydrase (CA). The kinetics of the hydration process was described by the equation:

$$v = a(k_u \cdot [CO_2] - \frac{k_v}{K}[H^+]\cdot[HCO_3^-],$$

where a – is a parameter that determines the reaction activation level with the participation of CA. $k_u = 0{,}137\ s^{-1}$, $k_v = 57.5\ s^{-1}$, $K = 0.35\,mM$ (Bidani et al., 1978; Geers & Gros, 2000), a = 1 is for a non-enzymatic process, a = 1000 is for the intracellular reaction catalyzed by CA (established in the simulation process).

b) The flux CO_2 was described by the reverse process $CO_2\_in \underset{k_2}{\overset{k_1}{\rightleftarrows}} CO_2\_out$, as in work (Geers et al., 2000; Al-Samir et al., 2013; Michenkova et al., 2021). The rate of the process was described by the equation: $v = k_1 \cdot [CO_2]_{in} - k_2 \cdot [CO_2]_{out}$, where $k_1 = k_2 = 0.93 \cdot 10^{-3}\ s^{-1}$ (set during simulation).

c) binding of CO_2 to oxy-, deoxyhemoglobin was described by the reaction:

$$n\,CO_2 + Hb \cdot NH_2 \underset{K_c}{\overset{k_a}{\rightleftarrows}} Hb \cdot NHCOO^- + H^+.$$

The rate of the reaction was described Geers & Gros (2000):

$$v_{oxyHb} = k_{a\_oxy} \cdot \left([oxyHb] \cdot z_0 - [carbHb]\right),$$

$$v_{deoxyHb} = k_{a\_deoxy} \cdot \left([deoxyHb] \cdot z_r - [carbHb]\right),$$

where $z_0 = \dfrac{2 \cdot [CO_2]_{in}}{4 \cdot \left([CO_2]_{in} + \dfrac{[H^+]_{in}}{K_{c,oxy}} + \dfrac{[H^+]_{in}^2}{K_{c,oxy} \cdot K_{z,oxy}} \right)}$,

$$z_r = \frac{2 \cdot [CO_2]_{in}}{4 \cdot \left(\dfrac{1}{\left([CO_2]_{in} + \dfrac{[H^+]_{in}}{K_{c,\alpha\_deoxy}} + \dfrac{[H^+]_{in}^2}{K_{c,\alpha\_deoxy} \cdot K_{z,\alpha\_deoxy}} \right)} + \dfrac{1}{\left([CO_2]_{in} + \dfrac{[H^+]_{in}}{K_{c,\beta\_deoxy}} + \dfrac{[H^+]_{in}^2}{K_{c,\beta\_deoxy} \cdot K_{z,\beta\_deoxy}} \right)} \right)},$$

where Kz and Kc – are the respective equilibrium constants, k_a – is the forward rate constant for reaction. It is known that the values of the constants K_z and K_c (and possibly k_a) are different depending on the oxygenation level of hemoglobin and 2,3-DPG. Thus, binding of CO_2 to α- and β-chains of deoxyhemoglobin in the presence of 2,3-DPG was described with n = 2, pKz(α) = 7.32, pKz(β) = 6.35 and pKc(α) = 5.04, pKc(β) = 4.39. The binding of CO_2 to α-chains of oxyhemoglobin was described with n = 2, pKz = 6.72 and pKc = 5.58 (Geers & Gros, 2000, Rees et al., 2010). The value of the rate constant $k_{a\_deoxy} = k_{a\_oxy} = 1\ M^{-1}\ s^{-1}$ (established based on simulation results).

Bicarbonate ion. The mass balance of bicarbonate ions in each compartment is determined by the hydration-dehydration reaction rate expression, and the flux of HCO^{3-} through the erythrocyte membrane. The model considered the exchange flux of HCO_3^- with the participation of band 3 protein (AE1), which acts as an anion exchanger.

The transport of HCO^{3-} through the AE1 transporter was described by the reverse process $HCO_3^-\_out \underset{k_2}{\overset{k_1}{\rightleftarrows}} HCO_3^-\_in$.

The exchange of HCO^{3-} for Cl^- was described in the paper in terms of passive diffusion along an electrochemical gradient:

$$v = k_1 \cdot [HCO_3^-]_{out} - \frac{k_2 \cdot \left(1 + 10^{pHi - pKa}\right)}{1 + \dfrac{10^{pHi - pKa}}{r}} [HCO_3^-]_{in},$$

$k_1 = k_2 = 6{,}9 \cdot 10^{-6}\ s^{-1}$ (established in the simulation process), $pKa = 6.3$, r – the Donnan ratio, $r = \dfrac{[HCO_3^-]_{in}}{[HCO_3^-]_{out}} = 0{,}69$. The HCO_3^- transfer of across the cell membrane approaches the intracellular concentration of HCO_3^-, that is not equal to the extracellular concentration, but is in Donnan equilibrium (Geers & Gros, 2000; Nishino et al., 2013). The condition of maintaining of the Donnan distribution for HCO_3^- leads to that the HCO_3^- uptake of is accompanied by a CO_2 flux (Al-Samir et al., 2013), or binding to the formation of carbhemoglobin.

Chloride ion. The Cl^- ions flux of was not considered in this version of the model. The concentration of chloride ions in the environment and in erythrocytes changes only with the Cl^- flux across the cell membrane in exchange for HCO_3^-. Therefore, the Cl^- flux across the erythrocyte membrane is equal and opposite to that for HCO_3^- (Bidani et al., 1978).

Hydrogen ions. The H^+ changes in cells occur due to hydration-dehydration of CO_2, association-dissociation of hemoglobin and carbamate, oxygenation-deoxygenation of hemoglobin (the last two processes occur only intracellularly). When 1 mol of CO_2 is hydrated, 1 mol of H^+ is formed. According to the literature, the moles of H^+ released per mole of CO_2 bound by hemoglobin (QH^+/carbamate) range from 1 to 2 (Bidani et al., 1978). Oxygenated hemoglobin is a stronger acid than deoxygenated hemoglobin, also H^+ are released from hemoglobin during oxygenation. According to data (Bidani et al., 1978), at normal levels of 2,3-DPG, 0.7 mol of H^+ is released per mol of HbO_2 formed under normal physiological conditions. Thus, the actual change in free intracellular H^+ is due to the balance between its production and consumption and the action of intracellular buffers, mainly hemoglobin.

Buffer cellular reactions. Buffering of protons by hemoglobin occurs according to the reactions:

$$bH^+ + Hb \cdot NH_2 \underset{K_c}{\overset{k_a}{\rightleftarrows}} Hb \cdot NH_3^+,$$

$$bH^+ + HbO_2 \cdot NH_2 \underset{K_c}{\overset{k_a}{\rightleftarrows}} HbO_2 \cdot NH_3^+$$

The rate of the process was described: $v = k_a \cdot [A] \cdot [H^+]_{in}^b - k \cdot K_c \cdot [C]$, A – oxyHb, deoxyHb, C – protonated form of oxyHb or deoxyHb, k_a – protonation constant, $k_{deoxyHb} = 90\,M^{-1} \cdot s^{-1}$, $k_{oxyHb} = 21 M^{-1} \cdot s^{-1}$, K – dissociation constant of the certain form of hemoglobin ($K_{deoxyHb} = 1.581 \cdot 10^{-8}$ ($pKa = 7.8$), $K_{oxyHb} = 2.51 \cdot 10^{-7}$ ($pKa = 6.6$), $b_{oxyHb} = 1$, $b_{deoxyHb} = 3$).

The model does not have a cycle of adenylate metabolism, which can affect the simulation results.

Calculations according to the model. Estimation of the parameters of the models. The mathematical model allows you to create a procedure for comparing experimental data, which are the time dependences of the pHi change and *a priori* ideas about the flow pattern of the process of interactions in a complex system. This makes it possible to find some unknown parameters of the model. The search for the numerical values of some kinetic parameters included in the reaction rate equation, as well as the initial values of intracellular CO_2 and HCO_3^- was carried out based on the condition of the best match of the experimental and calculated dependences of the pHi values obtained in kinetic experiments during the solution of the systems of equations included to the model.

The task was solved using search optimization methods. Parameter estimation is a special case of the optimization problem, in which an attempt is made to find a set of model parameter values at which the distance between model behaviour (simulation results) and experimental data is minimized. COPASI provides some parameter estimation functionality that is based on optimization methods (Mendes et al., 2009). COPASI measures the distance between theoretical (obtained by simulation) and experimental data using an expression derived from the least squares method. The objective function has the form:

$$O(p) = \sum_j \sum_k \left(pH_{k,j} - pH_{k,j}(p) \right)^2,$$

where $pH_{k,j}$ – is the experimental *pHi* value at measurement j within experiment k and the corresponding simulated data point is given by $pH_{k,j}(p)$, where p – is the vector of parameter values, used for the simulation (Mendes et al., 2009).

In the paper, the search for parameters is performed using the Evolutionary Programming method. The result of parameters' estimation procedure is a set of kinetic parameters characterizing the speed of each process in the system.

Time course procedure. The results of time course procedure are:

– families of kinetic curves describing the time dependence of substrates and products for the studied system,

– families of kinetic curves characterizing the flow of relevant processes and their changes over time.

Experimental studies. The protocol of the experimental part of the study complies with the principles of biological ethics and was approved by the Local Ethics Committee of the Vasyl Stus Donetsk National University, Faculty of Chemistry, Biology and Biotechnology (Vinnytsia, Ukraine). The experiments used fresh blood from donors of approximately the same age group and the same sex. Erythrocytes were separated

from plasma by centrifugation and washed three times with Na-phosphate buffer (0.015 M, pH 7.4) (buffer solution 1) containing 0.15 M NaCl (cells *a*). To obtain erythrocytes with a reduced initial value of intracellular pHi (cells *b*), additional washing with Na-phosphate buffer (0.015 M, pH 7.4) was used (Meryman & Hornblower, 1991).

In the obtained erythrocyte paste, the total hemoglobin content was determined by the hemoglobin cyanide unified method using a standard kit. The resulting paste of erythrocytes was introduced into the medium of the same buffer solution without glucose content. The hemoglobin content in the studied suspensions was at the level of 3.00 ± 0.18 mg/mL. pHi was studied in hemolysates of erythrocytes before the start of the experiment and then every 20 min during incubation in buffer solution 1. During the experiment, the system under study was in contact with ambient air. After certain time intervals, 2 mL of erythrocyte suspension was taken into a test tube and subjected to centrifugation at 3000 rpm for 1 min. The supernatant was carefully aspirated, the cells were lysed by adding 1 mL of deionized water. The pH measurement was performed using a laboratory ionomer using a combined electrode (ESK-10614/7) (Nishino et al., 2013). The experiments were carried out at a temperature of 25 °C in three to five replicates (n).

The results were analyzed in the Statistica 8.0 program (StatSoft Inc., USA). Experimental data are presented as x ± SE (x is the mean, SE is standard error of mean).

Results

The initial values of intracellular concentrations of CO_2 and HCO_3^- were obtained using the parameter optimization procedure. Values were in case (a) 6.2 ± 1.7 and 231.1 ± 68.7 μM, and in case (b) 42.6 ± 8.7 and 298.9 ± 47.7 μM respectively. The content of dissolved CO_2 and HCO_3^- was considered fixed at the level of 8.38 and 168.8 μM (calculated according to the Henderson-Hasselbach equation). It was believed that the extracellular medium pH did not change and was 7.4.

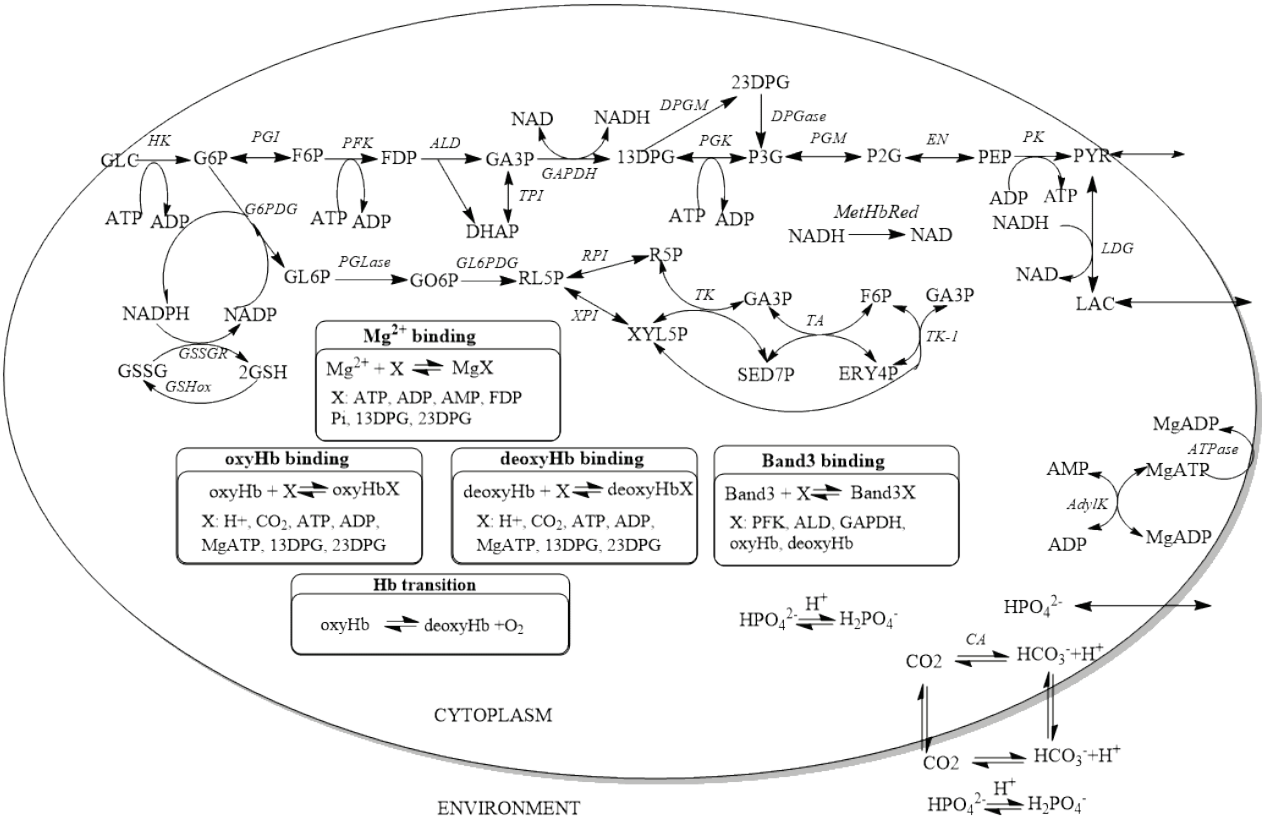

Fig. 1. Pathways reaction involved in the model: adapted from Nishino et al. (2013);
abbreviations for metabolites: 13DPG, 1,3-biphosphoglycerate, 23DPG, 2,3-diphosphoglycerate, DHAP, dihydroxyacetone phosphate, ERY4P, erythrose 4-phosphate, F6P, fructose-6-phosphate, FDP, fructose diphosphate, G6P, glucose-6-phosphate, GA3P, glyceraldehydes-3-phosphate, GL6P, 6-phosphogluco lactone, GLC, glucose, GO6P 6-phosphogluconate, GSH, reduced glutathione, GSSG, oxidized glutathione, LAC, lactate, P2G, 2-phosphoglycerate, P3G, 3-phosphoglycerate, PEP, phosphenolpyruvate, PYR, pyruvate, R5P, ribose-5-phosphate, RL5P, ribulose-5-phosphate, SED7P, sedoheptulose 7-phosphate, XYL5P, xylose-5-phosphate; abbreviations for reactions: AdylK, adenylate kinase (EC 2.7.4.3), ALD, aldolase (EC 4.1.2.13), DPGase, diphosphoglycerate phosphatase (EC 3.1.3.13), DPGM, diphosphoglycerate mutase (EC 5.4.2.4), EN, enolase (EC 4.2.1.11), G6PDH, glucose-6-phosphate dehydrogenase (EC 1.1. 1.49), GAPDH, glyceraldehyde-3-phosphate dehydrogenase (EC 1.2.1.12), GL6PDH, phosphogluconate dehydrogenase (EC 1.1.1.44), GSSGR, glutathione-disulfide reductase (EC 1.8.1.7), HK, hexokinase (EC 2.7.1.1), LDH, lactate dehydrogenase (EC 1.1.1.27), MetHbRed, methemoglobin reductase, MT, PFK, phosphofructokinase (EC 2.7.1.11), PGI, glucose-6-phosphate isomerase (EC 5.3.1.9), PGK, phosphoglycerate kinase (EC 2.7.2.3), PGLase, phosphogluconolactonase (EC 3.1.1.31), PGM, phosphoglycerate mutase (EC 5.4.2.1), PK, pyruvate kinase (EC 2.7.1.40), PRM, phosphoribomutase (EC 5.4.2.7), RPI, ribose-5-phosphate isomerase (EC 5.3.1.6), TA, transaldolase (EC 2.2.1.2), TK, transketolase (EC 2.2.1.1), TPI, triosephosphate isomerase (EC 5.3.1.1), XPI, ribulose phosphate epimerase (EC 5.1.3.1)

The results of measuring pH in erythrocytes that were washed in buffer medium 1 and then incubated in this medium for 3 hours are shown in Figure 2. The pHi change in erythrocytes with their initial value 7.12 ± 0.05 is shown in Figure 2a. The pHi change in erythrocytes with their initial value 7.05 ± 0.04 is shown in Figure 2b. It is evident that manipulation with cells violates the stationary pH value to varying degrees, but over time, restoration to equilibrium value take place. The nature of the pH change during the first hour of incubation is different and depends on the CO_2 content in the cells. The solid line is the pH dependence obtained during the model's parameter optimization (parameter estimation) followed by the solution of the model's differential equations (time course procedure). The model predicts a sharp increase in pHi in the condition a, and a sharp decrease in condition b within 1 s from the start of the experiment. The following Figures 3–7 show the information obtained during the simulation.

The coincidence of experimental and calculated values of pHi allows us to claim that the simulation results reflect real processes in cells.

The flux through CA in cells a and b is shown in Figure 3. In cells a, after their introduction into the incubation medium, the flux through CA varied from –120.9 μM/s (CA consumed HCO_3^- and H^+ and produced CO_2) to –0.096 μM/s. After 1.3 s, the flux changed its sign and reached the level of 1.2 μM/s, after which it rapidly decreased (Fig. 3a). After 2 min, the flow through the CA reached the level of 0.069 μM/s and further decreased very slowly. In cells b, the initial flow through CA was 1.3 μM/s. The calculated values of the flows through CA are much lower, but the nature of the changes is similar to condition a (Fig. 3b). After 60 min of the experiment, the magnitudes of currents through CA in cells a and b did not differ.

The results of modeling the dynamics of CO_2 and HCO_3^- content are shown in Figure 4. In the case of a cells, the initial value of CO_2 in the cells is 2.15 μM and HCO_3^- 227.56 μM. In 1.3 s, CA reduces HCO_3^- to 184 μM (Fig. 4a), while the content of CO_2 increases only by 2.32 μM. In b cells, the initial content of CO_2 was 33 μM and HCO_3^- 245.85 μM. Due to the high concentration of CO_2, CA converts CO_2 to HCO_3^-, as a result of which its concentration decreases for 7 minutes (Fig. 4b) and the content of HCO_3^- increases. After 60 minutes of the experiment, the predicted values of the content of CO_2 and HCO_3^- in cells a and b differed slightly, and for 180 minutes there was an increase in the intracellular content of both CO_2 and HCO_3^-.

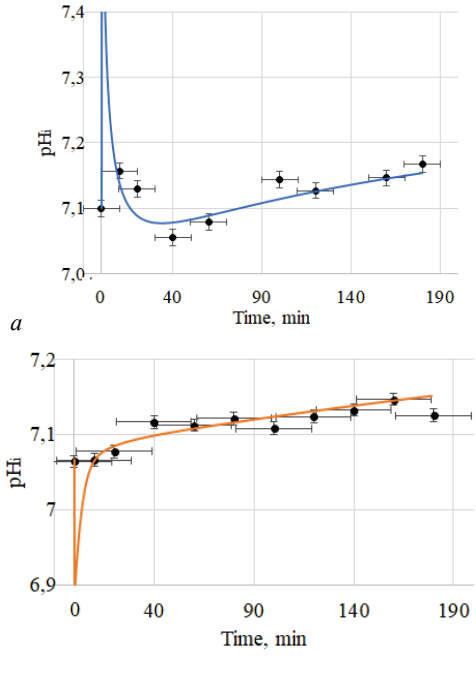

Fig. 2. Erythrocytes pHi changes in during incubation in Na-phosphate buffer (0.015 M, pH 7.4) containing 0.15 M NaCl with pHi0 7.12 ± 0.05 (a) and 7.05 ± 0.04 (b); each point is represented as x ± SE, n = 5; the solid line is time courses of computed changes pHi

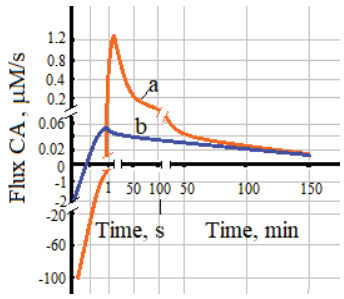

Fig. 3. Fluxes across CA according to simulation results in cells during incubation: cells *a* – orange dependency, *b* – blue

Fluxes of CO_2 and HCO_3^- across the channels and exchanger AE1 are shown in Figure 5. The fluxes' sign is showing its direction (according to how the process is described in the model (Table 1)). A positive flux of CO_2 means its outflow from the cell, a positive flux of HCO_3^- means an influx of HCO_3^- into the cell from the outside. In cells a, during 1.3 s, CO_2 and HCO_3^- enter, during the same period, the fluxes into the cell decrease, and after 1.3 s, the outward fluxes of CO_2 and HCO_3^- become dominant. From the beginning of the experiment, CO_2 and HCO_3^- fluxes outward from cells b.

The total H^+ fluxes of hemoglobin-involved buffering processes are shown in Figure 6. Figure 7 shows changes in the content of carbhemoglobin in cells. In a cells for 1.3 s it is oxyhemoglobin which is the donor of H^+ for CA (data not shown) which during this time interval converts HCO_3^- into CO_2. The processes of H^+ binding are significantly reduced (Fig. 6a) and a significant amount of the formed CO_2 binds to hemoglobin (Fig. 7a). After 1.3 s CA begins to catalyze the CO_2 hydration reaction, which leads to acidification of the internal environment (Fig. 2a). An increase in H^+ content shifts the carbamination reaction towards dissociation, the level of carbamate in cells decreases, and CO_2 increases. This could be explained by higher flux across CA in the 1–50 s time interval in cells a. CO_2 is hydrated by CA and removed from the cell.

In cells b, there is an excess of CO_2, which is immediately converted by CA into HCO_3^- and H^+. Subsequently there is a need to bind H^+, which is indicated by an increase in the flux across the buffer systems. After 25 minutes, H^+ binding fluxes in both cell types become the same and then tend to decrease. In cells b, the level of carboxyhemoglobin slowly gradually increases (Fig. 7b).

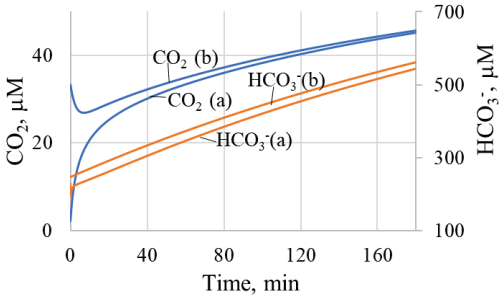

Fig. 4. CO_2 and HCO_3^- content (μM) in erythrocytes during the incubation time according to the simulation results

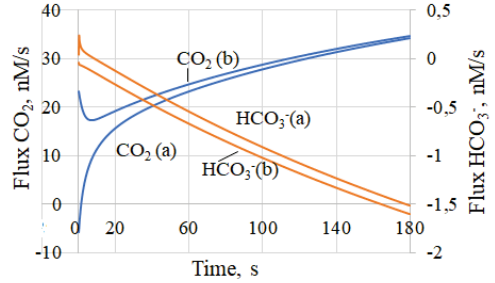

Fig. 5. CO_2 and HCO_3^- fluxes (μM/s) during the incubation time according to the simulation results

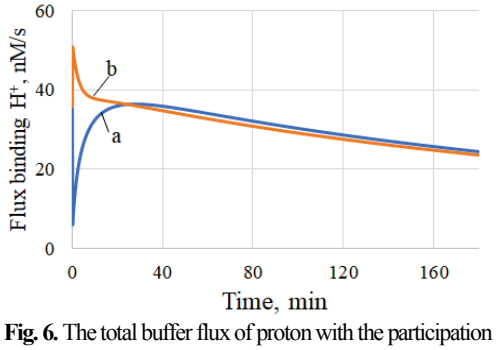

Fig. 6. The total buffer flux of proton with the participation of hemoglobin in cells a and b according to the simulation results

A schematic representation of the processes involved in the restoration of the steady-state value of pHi in cells a is shown in Figure 8. The restoration of the steady-state value of pHi in cells b corresponds to

the scheme in Figure 8c. A detailed discussion of these mechanisms is provided in the Discussion section.

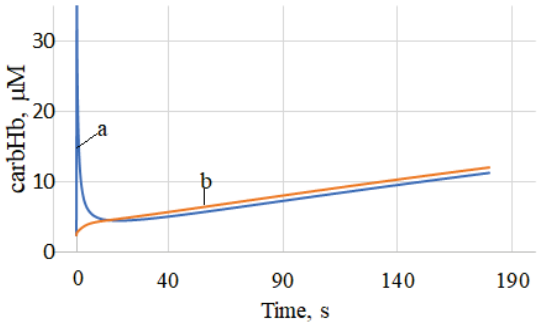

Fig. 7. Carbhemoglobin content (μM) in cells a and b according to simulation results

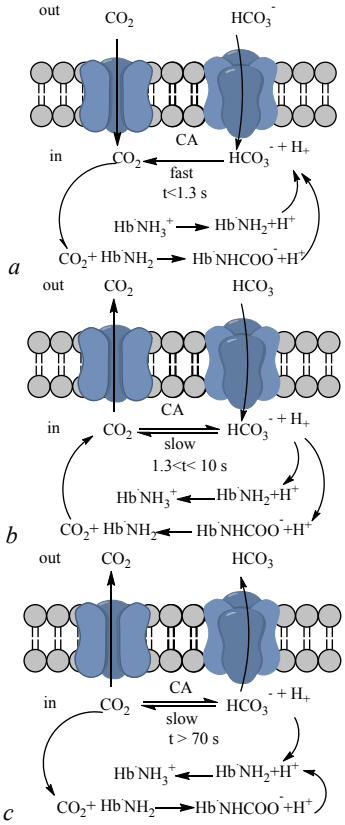

Fig. 8. Schematic diagrams of mechanism restoration of the steady-state value of pHi in cells a: $a - t < 1.3$ s, $b - 1.3 < t < 10$ s, $c - t > 70$ s

Discussion

In the cytosol, pH is both one of the most controllable and one of the most difficult parameters to control. The pH of the medium determines the degree of protonation of acid-base groups, which are especially abundant in macromolecular aggregates. Since enzymes and cellular metabolites exhibit a strong dependence on pH, modifying the protonation of key residues can profoundly affect primarily the surface charge of macromolecules. Thus, pHi regulation is based on an intricate interaction between the large number of protonated groups in biological molecules, pKa values, expression parameters, stability, kinetics, and affinity of pH regulation systems (Bouret et al, 2014). The regulation of pHi depends on the opposite actions of enzymes and transporters in the plasma membrane, capable of both increasing and decreasing pHi (Occhipinti & Boron, 2015; Occhipinti & Boron, 2019). In the absence of good mathematical models, it is very difficult to discern the relative contributions of the many simultaneous and interconnected processes responsible for pH changes in a single living cell.

Table 1
Some reactions in erythrocyte metabolism included in the model and corresponding catalyzing enzymes (Arrow type, → or ↔ indicates irreversible or reversible reactions)

Reactions	Enzymes	Effectors
Glycolysis		
Glc + MgATP → G6P + MgADP	HK	23DPG, GDP, GSH, pH
G6P ↔ F6P	PGI	–
F6P + ATP → FDP + ADP	PFK	ATP, Mg, 23DPG, AMP, Phos
FDP ↔ GA3P + DHAP	ALD	23-DPG, Mg23DPG
DHAP ↔ GA3P	TPI	–
GA3P + NAD^+ ↔ D13PG + NADH	GAPDH	pH
13DPG + ADP ↔ P3G + ATP	PGK	–
P3G ↔ P2G	PGM	–
P2G ↔ PEP	EN	Mg
PEP + ADP → PYR + ATP	PK	ATP, F16DP
PYR + NADH → LAC + NAD^+	LDG	pH
PYR ↔ PYRext	transpot	–
LAC ↔ LACext	transpot	pH
Phos ↔ Phosext	transpot	pH
2,3-bisphosphoglycerate shunt		
D13PG → D23PG	DPGM	pH
D23PG → P3G	DPGase	–
Pentose phosphate pathway		
G6P + NADP → GL6P + NADPH	G6PDH	MgATP, 23DPG
GL6P ↔ GO6P	PGLase	–
GO6P + NADP → RL5P + NADPH	GL6PDH	–
RL5P ↔ XYL5P	XPI	–
RL5P ↔ R5P	RPI	–
XYL5P + R5P ↔ SED7P + GA3P	TK-1	–
SED7P + GA3P ↔ F6P + ERY4P	TA	–
XYL5P + ERY4P ↔ F6P + GA3P	TK	–
GSSG + NADPH ↔ GSH + NADP	GSSGR	–
GSH → GSSG	GSHox	–
MgATP → MgADP + Phos	ATPase	–
NADH → NAD	non-glycolytic NADH consumption process	
Jacobs-Stewart cycle		
$CO_2 + H_2O \leftrightarrow HCO_3^- + H^+$	CA	–
$CO_2 \leftrightarrow CO_2$ext	transport	–
$HCO_3^- \leftrightarrow HCO_3^-$ext	transport	–
Binding of metabolites to hemoglobin		
deoxyHb+13DPG ↔ deoxyHb13DPG	–	pH
deoxyHb+23BPG ↔ deoxyHb23DPG	–	pH
deoxyHb + ATP ↔ deoxyHbATP	–	pH
deoxyHb + ADP ↔ deoxyHbADP	–	pH
deoxyHb + FDP ↔ deoxyHbFDP	–	pH
deoxyHb + MgATP ↔ deoxyHbMgATP	–	pH
deoxyHb + H^+ ↔ H deoxyHb	–	–
deoxyHb + CO_2 ↔ deoxyHbCO_2 + H^+	–	–
oxyHb+13DPG ↔ oxyHb13DPG	–	pH
oxyHb+23DPG ↔ oxyHb23DPG	–	pH
oxyHb + ATP ↔ oxyHbATP	–	pH
oxyHb + ADP ↔ oxyHbADP	–	pH
oxyHb + FDP ↔ oxyHbFDP	–	pH
oxyHb + MgATP ↔ oxyHbMgATP	–	pH
oxyHb + H^+ ↔ HoxyHb	–	–
oxyHb + CO_2 ↔ oxyHbCO_2 + H^+	–	–
Hemoglobin transition		
deoxyHb + O_2 ↔ oxyHb	–	pH, CO_2, T
Binding of metabolites to band3 protein		
Band3+ALD ↔ Band3ALD	–	–
Band3+GAPDH ↔ Band3GAPDH	–	–
Band3+PFK ↔ Band3PFK	–	–
Band3+LDG ↔ Band3LDG	–	–
Band3+deoxyHb ↔ Band3deoxyHb	–	–
Band3+oxyHb ↔ Band3oxyHb	–	–

In this study, a metabolic model of erythrocytes is presented, which makes it possible to quantitatively evaluate acid-base transformations in

erythrocytes as a response to the action of the external environment. The model of human erythrocyte metabolism (Mulquiney & Kuchel, 1999) was chosen as the basis, consisting of two metabolic cycles – glycolysis and the pentose phosphate pathway. The advantage of this model is that the rate of most reactions is described as a function of pH. To this model, we add metabolic processes involving hemoglobin, namely, interactions with cell metabolites, binding to band 3 protein, oxygenation processes, the Jacobs-Stewart cycle, using the currently known kinetic equations and their parameters (Bidani et al., 1978; Geers & Gros, 2000; Kinoshita et al., 2007; Nishino et al., 2013). The combination of all these processes in one model is crucial, since hemoglobin, 2,3-DPG and other cellular metabolites directly or indirectly affect pH. The procedure of optimization parameters search (parameter estimation) followed by the solution of differential equations of the model (time course procedure) was used to predict the behaviour of all measured and non-measurable variables over time. At this stage, the model is used for the analysis of experimental data on changes in the pH of erythrocytes during their incubation in a buffer solution and the study of the mechanisms of pH regulation in cells.

According to the simulation results, regulation of pH in erythrocytes placed in a buffer medium takes place with the participation of two types of processes – fast (passing in 1.3 s) and slow. As it was established, CA is responsible for fast processes. The driving force behind the rapid process is the difference between the CO_2 concentration and the value $\frac{k_v \cdot [H^+] \cdot [HCO_3^-]}{K \cdot k_u}$. In cells a, the difference between these indicators is 19.56 μM. Equilibrium is restored in the reaction $CO_2 + H_2O \underset{kv}{\overset{ku}{\rightleftarrows}} H_2CO_3 \overset{K}{\rightleftarrows} H^+ + HCO_3^-$ in 1.3 s. The flux across carbonic anhydrase at t = 0.1 s is –120.9 μM/s (CA consumes HCO_3^- and H^+ and produces CO_2), at t = 1.3 s the flow through CA is already –0.096 μM/s (Fig. 3a). During this time $[CO_2] = \frac{k_v \cdot [H^+] \cdot [HCO_3^-]}{K \cdot k_u}$. According to the simulation results, the high speed of this reaction is ensured by hemoglobin, which supplies the greater part of the consumed H^+ (Fig. 6a, 8a). At the same time, a significant amount of the formed CO_2 is utilized in the form of carbhemoglobin (Fig. 7a, 8a), and not with the participation of gas channels (Occhipinti & Boron, 2015). As a result, the content of cellular CO_2 increases only from 2.16 to 2.31 μM. The payment for equilibrium is a rapid rise in pH.

In the case of cells *b*, the content of CO_2 and the value $\frac{k_v \cdot [H^+] \cdot [HCO_3^-]}{K \cdot k_u}$ are balanced (initial content of CO_2 33.3 μM). The modeling results indicate the absence of fast processes (Fig. 3b), the flow through the CA is slow. In this case, CA catalyzes the CO_2 hydration reaction. Excess H^+ is mainly bound by deoxyhemoglobin (Fig. 6b). Calculations predict a decrease in pH, but this decrease is less than 0.1 pH.

According to the simulation results, after 1.3 s the equilibrium establishing processes for H^+ start. The equilibrium condition for H^+ is the Donnan condition, meaning H^+ must be transferred into the cell. In the case of b cells, the opposite is true. The Jacobs-Stewart cycle ensures slow processes of establishing equilibrium (Swietach et al., 2010; Jennings, 2013). The speed of this cycle is clearly limited by the slow hydration-dehydration reactions, with the participation of CA and the transport of CO_2 and HCO_3^-. The relative deficiency of H^+ inside the cells leads to intracellular hydration of CO_2 (Fig. 3a, dependence of the flow through CA in the positive region). The formed excess HCO_3^- diffuses from erythrocytes through band 3 dimers (AE1) or dimerized dimers (tetramers) along the electrochemical potential gradient in exchange for chloride (reverse chloride shift) (Reithmeier et al., 2016; Jennings, 2021). The decrease in pHi, which is recorded experimentally (Fig. 2a), may be explained by the fact that since along with HCO_3^-, H^+ is also formed. An increase in the level of H^+ causes the dissociation of carbhemoglobin, and already here the excess CO_2 is removed through gas channels (Fig. 8b). In general, the processes that allow restoring the level of intracellular pH as shown in Figures 8b, 8c.

Carbonic anhydrase is the most efficient enzyme known to date, with a kcat or turnover number (~6×10^5/s) that is 10 times faster than the rate of Cl^-/HCO_3^- exchange carried out by AE1 (~5×10^4 ions/s) (Boone et al., 2014; Hsu, 2018; Kalli & Reithmeier, 2022). Since human erythrocytes have an identical number of CAII and AE1 molecules (~10^6 molecules/erythrocyte), the efficiency of CO_2/ HCO_3^- conversion with the participation of CA is about an order of magnitude higher than the rate of Cl^-/HCO_3^- – exchange flow with the participation of AE1. It is known that CA is present in erythrocytes in two isoforms: low-affinity, high-capacity enzyme (CAI) and high-affinity, low-capacity isoenzyme (CAII). It is suggested that cytosolic carbonic anhydrase II (CAII) of erythrocytes is highly associated with AE1, forming a "metabolon complex" that significantly enhances the transport activity of AE1 (Boron, 2010; Johnson & Casey, 2011; Al-Samir et al., 2013; Occhipinti & Boron, 2015; Hsu, 2018). Recently, an aquaporin (AQP1) has also been shown to spatially associate with CAII and transport H_2O for CAII-mediated catalysis (Vilas et al., 2015; Hsu, 2018; Michenkova et al., 2021). Nevertheless, the formation of metabolon seems doubtful to some authors (Al-Samir et al., 2013).

The results obtained while modeling indicate that the rapid conversion of HCO_3^- to CO_2 with the participation of CA is ensured simultaneously by the hemoglobin participation processes. The binding of hemoglobin to the band protein is well established (Chu et al., 2016; Kosmachevskaya et al., 2019; Giardina, 2022). Deoxygenated hemoglobin (deoxyHb) preferentially binds to the N-terminal cytoplasmic domain of band 3 protein. The catalytic dehydration reaction, which consumes protons to form CO_2, can only proceed under the conditions of availability of a sufficient number of protons. Protons bound to hemoglobin and the delivery of protons from the interior of the cell to the membrane region by diffusion of H^+ becomes the limiting step. The same applies to the binding of CO_2, which is formed in significant quantities during the conversion of HCO_3^- to CO_2. Hemoglobin binds CO_2 and releases H^+. From this point of view, colocalization of CA with hemoglobin and aquaporin could maximize the rate of dehydration and transport of HCO_3^- and CO_2. Metabolon formation can be viewed as a temporally extended CAII mechanism that is built on transient interactions between four proteins: AQP1, AE1, CAII, and deoxyHb.

One of the oldest mechanisms that provide a quick response to external influences is the ability of molecules to reversibly bind to membrane components (Kosmachevskaya et al., 2019). In erythrocytes, an example of feedback is the O_2-dependent association of hemoglobin with band 3 protein, which regulates the assembly of a complex of glycolytic enzymes on the erythrocyte membrane when the glucose level changes, switches the metabolism between the pentose phosphate pathway and glycolysis (Kosmachevskaya et al., 2019; Issaian et al., 2021). However, interactions with AE1 inhibit, rather than stimulate, the activity of glycolytic enzymes. Boron (2010) suggests that in the case of large intracellular gradients for Na^+, HCO_3^-, H^+ ions, the distribution of CAII throughout the cytoplasm helps to quickly dissipate the ion gradient and thereby enhance particle transport. Here we see the need for further development of the model, modeling of CAII binding to AE1, and detailed analysis of the role of membrane-bound and cytoplasmic hemoglobin in the work of CAII.

During the search optimization of the model parameters (Parameter Estimation), the diffusion rate constant $0.93 \cdot 10^{-3}\ s^{-1}$ was obtained, which is two orders of magnitude higher than that proposed in the literature for CO_2 diffusion. If we consider that ~60% of CO_2 flow into or out of erythrocytes occurs through the gas channel AQP1 (Hsu, 2018; Michenkova et al., 2021), then the use of this constant is more appropriate. The rest of the CO_2 flux likely occurs through another gas channel, RhAG, or direct diffusion across the lipid bilayer.

An interesting point that was shown during the simulation is a short-term increase/decrease in pH during the operation of the CA. This fact was also pointed out by other authors (Boron, 2010; Occhipinti & Boron, 2019). Thus, in experiments with oocytes (Musa-Aziz et al., 2014) it was shown that cytosolic CA II increases the rate of change of both intracellular pHi and pH near the outer surface of the cell when CO_2 enters. Evidence for the formation of cytosolic H^+ gradients has been found in other cells (Johnson & Casey, 2011). The combination of fast AE1-mediated HCO_3^- transport and slow H^+ diffusion creates conditions for the formation of H^+ microdomains that develop around AE1. Thus, proteins near

AE1 will be exposed to a different pH than proteins further away from AE1. In turn, this can lead to differential regulation of pH-sensitive processes localized in the environment of pH-regulatory transporters. CAII localizes to the cytosolic C-terminus of AE1 (De Rosa et al., 2007; Johnson & Casey, 2011), the site of H^+ production or consumption is also localized to the surface of AE1, contributing to the formation of the H^+ microdomain. The N-terminus of AE1 contains binding sites for glycolytic enzymes (Chu et al., 2016; Issaian et al., 2021), whose activity depends on pH. It is logical to hypothesize that enzymes may localize to the surface of AE1 to undergo pH regulation by H^+ microdomains. Experimental data on the effect of pH on the glycolytic and pentose phosphate pathways in erythrocytes are given in Huang et al. (2021). This is another argument for the feasibility of forming metabolon CA, AQP1 from AE1.

Since the protons produced by bicarbonate formation are released in the immediate vicinity of band 3, the Bohr release of oxygen occurs most rapidly from hemoglobin in the same region. Thus, the structural organization of the band 3 macrocomplex appears to be well formed to fulfill this special requirement, providing short pathways for the movement of oxygen, carbon dioxide, protons, and bicarbonates necessary for efficient oxygen/carbon dioxide exchange in the capillaries, which would not occur if these processes were not physically connected (De Rosa et al., 2007).

Hemoglobin is an example of a molecule that is subject to modulation mechanisms that optimize its functional behaviour according to specific physiological requirements. Hemoglobin binds to band 3 protein due to the insertion of the anionic AE1 segment into the cationic central cavity formed by the central β-chains, which is also the 2.3-DPG binding site (De Rosa et al., 2007; Kosmachevskaya et al., 2019). AE1 stabilizes the T-conformation of hemoglobin, which has a high affinity for binding H^+, on the other hand, hemoglobin activates the anion-transporting properties of AE1 due to an increase in the content of HCO_3^- (Fig. 4, 5).

Carbamate formation and hemoglobin protonation are easily reversible reactions, which is a useful property for any biological regulation system (Lorimer, 1983). The buffer properties of hemoglobin are carried out by the imidazole group of histidine residues, which has a pKa of approximately 6.8, which provides effective buffering at physiological pH. The amount of CO_2 bound as a carbamate to hemoglobin in erythrocytes depends on the oxygen saturation of hemoglobin and the concentration of 2,3-DPG and the concentration of H^+ (Blake & Cann, 2022). However, the formation of a carbamate on a protein converts a neutral or cationic group into an anionic group with the addition of a relatively small mass equivalent to a 4 to 5 Å diameter sphere. This creates the possibility of electrostatic interactions within the protein that can further stabilize the carbamate. The formation of the carbamate as well as the T conformation of hemoglobin can lead to subtle conformational changes with profound biological consequences (Lorimer, 1983).

Conclusions

The developed model is a tool for the quantitative analysis of biochemical interactions important for the regulation of intracellular pH. The model does not consider metabolic cycles separately from one another, but, on the contrary, the Jacobs-Stewart metabolic cycle is integrated into a complex network of reactions, which allows one to consider most of the interrelationships between reactions. The model consists of 85 reactions, the rate of which is described based on exact kinetic equations. The result of the model's calculations are time dependences of reaction flows and metabolite concentrations, that allow one to reproduce the behaviour of the metabolic system after a disturbance *in vitro* and to establish the mechanisms of recovery or approach to stationary states.

The paper shows that regulation of pH in erythrocytes placed in a buffer medium takes place with the participation of two types of processes – fast (takes place in 1.3 s) and slow. Fast processes are aimed at restoring the intracellular balance between CO_2 and HCO_3^-, slow processes are aimed at establishing the balance of H^+ between the cell and the extracellular environment. The roles of carbonic anhydrase (CA) and hemoglobin in the processes of pH stabilization are shown and analyzed. The physiological role of the metabolon between band 3 protein (AE1), CA, aquaporin and hemoglobin in maintaining pH homeostasis in the conditions of *in vitro* experiments is discussed.

References

Al-Samir, S., Papadopoulos, S., Scheibe, R. J., Meißner, J. D., Cartron, J. P., Sly, W. S., Alper, S. L., Gros, G., & Endeward, V. (2013). Activity and distribution of intracellular carbonic anhydrase II and their effects on the transport activity of anion exchanger AE1/SLC4A1. The Journal of Physiology, 591(20), 4963–4982.

Bertocchio, J. P., Genetet, S., Da Costa, L., Walsh, S. B., Knebelmann, B., Galimand, J., Bessenay, L., Guitton, C., De Lafaille, R., Vargas-Poussou, R., Eladari, D., & Mouro-Chanteloup, I. (2020). Red blood cell AE1/Band 3 transports in dominant distal renal tubular acidosis patients. Kidney International Reports, 5(3), 348–357.

Bidani, A., Crandall, E. D., & Forster, R. E. (1978). Analysis of postcapillary pH changes in blood *in vivo* after gas exchange. Journal of Applied Physiology: Respiratory, Environmental and Exercise Physiology, 44(5), 770–781.

Blake, L. I., & Cann, M. J. (2022). Carbon dioxide and the carbamate post-translational modification. Frontiers in Molecular Biosciences, 9, 825706.

Boone, C. D., Pinard, M., McKenna, R., & Silverman, D. (2014). Catalytic mechanism of α-class carbonic anhydrases: CO_2 hydration and proton transfer. In: Frost, S., & McKenna, R. (Eds.). Carbonic anhydrase: Mechanism, regulation, links to disease, and industrial applications. Subcellular biochemistry. Springer, Dordrecht. Vol. 75, pp. 31–52.

Boron, W. F. (2010). Evaluating the role of carbonic anhydrases in the transport of HCO_3^--related species. Biochimica et Biophysica Acta, 1804(2), 410–421.

Bouret, Y., Argentina, M., & Counillon, L. (2014). Capturing intracellular pH dynamics by coupling its molecular mechanisms within a fully tractable mathematical model. PLoS One, 9(1), e85449.

Calvetti, D., Prezioso, J., Occhipinti, R., Boron, W. F., & Somersalo, E. (2020). Computational model of electrode-induced microenvironmental effects on pH measurements near a cell membrane. Multiscale Modeling and Simulation, 18(2), 1053–1075.

Chao, S. C., Wu, G. J., Huang, S. F., Dai, N. T., Huang, H. K., Chou, M. F., Tsai, Y. T., Lee, S. P., & Loh, S. H. (2018). Functional and molecular mechanism of intracellular pH regulation in human inducible pluripotent stem cells. World Journal of Stem Cells, 10(12), 196–211.

Chen, G. S., Lee, S. P., Huang, S. F., Chao, S. C., Chang, C. Y., Wu, G. J., Li, C. H., & Loh, S. H. (2018). Functional and molecular characterization of transmembrane intracellular pH regulators in human dental pulp stem cells. Archives of Oral Biology, 90, 19–26.

Cherif, A., Maheshwari, V., Fuertinger, D., Schappacher-Tilp, G., Preciado, P., Bushinsky, D., Thijssen, S., & Kotanko, P. (2020). A mathematical model of the four cardinal acid-base disorders. Mathematical Biosciences and Engineering, 17(5), 4457–4476.

Chu, H., McKenna, M. M., Krump, N. A., Zheng, S., Mendelsohn, L., Thein, S. L., Garrett, L. J., Bodine, D. M., & Low, P. S. (2016). Reversible binding of hemoglobin to band 3 constitutes the molecular switch that mediates O_2 regulation of erythrocyte properties. Blood, 128(23), 2708–2716.

De Rosa, M. C., Carelli Alinovi, C., Galtieri, A., Scatena, R., & Giardina, B. (2007). The plasma membrane of erythrocytes plays a fundamental role in the transport of oxygen, carbon dioxide and nitric oxide and in the maintenance of the reduced state of the heme iron. Gene, 398, 162–171.

Dotsenko, O. (2016). *In silico* modeling of the redox metabolism in human erythrocytes. Eureka: Life Sciences, 1, 39–46.

Doyen, D., Poët, M., Jarretou, G., Pisani, D. F., Tauc, M., Cougnon, M., Argentina, M., Bouret, Y., & Counillon, L. (2022). Intracellular pH control by membrane transport in mammalian cells. Insights into the selective advantages of functional redundancy. Frontiers in Molecular Biosciences, 9, 825028.

Geers, C., & Gros, G. (2000). Carbon dioxide transport and carbonic anhydrase in blood and muscle. Physiological Reviews, 80(2), 681–715.

Giardina, B. (2022). Hemoglobin: Multiple molecular interactions and multiple functions. An example of energy optimization and global molecular organization. Molecular Aspects of Medicine, 84, 101040–101045.

Hsu, K. (2018). Exploring the potential roles of band 3 and aquaporin-1 in blood CO_2 transport-inspired by comparative studies of glycophorin B-A-B hybrid protein GP.Mur. Frontiers in Physiology, 9, 733.

Huang, M., Liang, X., Zhang, Z., Wang, J., Fei, Y., Ma, J., Qu, S., & Mi, L. (2020). Carbon dots for intracellular pH sensing with fluorescence lifetime imaging microscopy. Nanomaterials, 10(4), 604.

Huang, Y. C., Cheng, M. L., Tang, H. Y, Huang, C. Y., Chen, K. M., & Wang, J. S. (2021). Eccentric cycling training improves erythrocyte antioxidant and oxygen releasing capacity associated with enhanced anaerobic glycolysis and intracellular acidosis. Antioxidants, 10(2), 285.

Issaian, A., Hay, A., Dzieciatkowska, M., Roberti, D., Perrotta, S., Darula, Z., Redzic, J., Busch, M. P., Page, G. P., Rogers, S. C., Doctor, A., Hansen, K. C., Eisenmesser, E. Z., Zimring, J. C., & D'Alessandro, A. (2021). The interactome of the N-terminus of band 3 regulates red blood cell metabolism and storage quality. Haematologica, 106(11), 2971–2985.

Jennings, M. L. (2013). Transport of H_2S and HS^- across the human red blood cell membrane: Rapid H_2S diffusion and AE1-mediated Cl^-/HS^- exchange. American Journal of Physiology, Cell Physiology, 305(9), C941–C950.
Jennings, M. L. (2021). Cell physiology and molecular mechanism of anion transport by erythrocyte band 3/AE1. American Journal of Physiology, Cell Physiology, 321, C1028–C1059.
Johnson, D. E., & Casey, J. R. (2011). Cytosolic H^+ microdomain developed around AE1 during AE1-mediated Cl^-/HCO_3^- exchange. The Journal of Physiology, 589, 1551–1569.
Kalli, A. C., & Reithmeier, R. A. F. (2022). Organization and dynamics of the red blood cell band 3 anion exchanger SLC4A1: Insights from molecular dynamics simulations. Frontiers in Physiology, 13, 817945.
Kinoshita, A., Tsukada, K., Soga, T., Hishiki, T., Ueno, Y., Nakayama, Y., Tomita, M., & Suematsu, M. (2007). Roles of hemoglobin allostery in hypoxia-induced metabolic alterations in erythrocytes: Simulation and its verification by metabolome analysis. Journal of Biological Chemistry, 282(14), 10731–10741.
Kosmachevskaya, O. V., Nasybullina, E. I., Topunov, A. F., & Blindar, V. N. (2019). Binding of erythrocyte hemoglobin to the membrane to realize signal-regulatory function (review). Applied Biochemistry and Microbiology, 55(2), 83–98.
Lee, D., & Hong, J. H. (2020). The fundamental role of bicarbonate transporters and associated carbonic anhydrase enzymes in maintaining ion and pH homeostasis in non-secretory organs. International Journal of Molecular Sciences, 21(1), 339–357.
Lew, V. L., & Bookchin, R. M. (1986). Volume, pH, and ion-content regulation in human red cells: Analysis of transient behavior with an integrated model. The Journal of Membrane Biology, 92(1), 57–74.
Leypoldt, J. K., Goldstein, J., Pouchoulin, D., & Harenski, K. (2020). Extracorporeal carbon dioxide removal requirements for ultraprotective mechanical ventilation: Mathematical model predictions. Artificial Organs, 44(5), 488–496.
Li, Y., Zhou, X., & Sun, S. X. (2021). Hydrogen, bicarbonate, and their associated exchangers in cell volume regulation. Frontiers in Cell and Developmental Biology, 9, 683686.
Lorimer, G. H. (1983). Carbon dioxide and carbamate formation: The makings of a biochemical control system Trends in Biochemical Sciences, 8(2), 65–68.
Lüscher, B. P., Vachel, L., Ohana, E., & Muallem, S. (2020). Cl^- as a bona fide signaling ion. American Journal of Physiology, Cell Physiology, 318(1), C125–C136.
Mendes, P., Hoops, S., Sahle, S., Gauges, R., Dada, J., & Kummer, U. (2009). Computational modeling of biochemical networks using COPASI. Methods in Molecular Biology, 500, 17–59.
Meryman, H. T., & Hornblower, M. (1991). Manipulating red cell intra- and extracellular pH by washing. Vox Sanguinis, 60(2), 99–104.
Michenkova, M., Taki, S., Blosser, M. C., Hwang, H. J., Kowatz, T., Moss, F. J., Occhipinti, R., Qin, X., Sen, S., Shinn, E., Wang, D., Zeise, B. S., Zhao, P., Malmstadt, N., Vahedi-Faridi, A., Tajkhorshid, E., & Boron, W. F. (2021). Carbon dioxide transport across membranes. Interface Focus, 11(2), 20200090.
Michl, J., Park, K. C., & Swietach, P. (2019). Evidence-based guidelines for controlling pH in mammalian live-cell culture systems. Communications Biology, 2, 144.
Mulquiney, P. J., & Kuchel, P. W. (1999). Model of 2,3-bisphosphoglycerate metabolism in the human erythrocyte based on detailed enzyme kinetic equations: Equations and parameter refinement. The Biochemical Journal, 342(3), 581–596.
Musa-Aziz, R., Occhipinti, R., & Boron, W. F. (2014). Evidence from simultaneous intracellular- and surface-pH transients that carbonic anhydrase IV enhances CO_2 fluxes across *Xenopus* oocyte plasma membranes. American Journal of Physiology, Cell Physiology. 307, C814–C840.
Nishino, T., Yachie-Kinoshita, A., Hirayama, A., Soga, T., Suematsu, M., & Tomita, M. (2013). Dynamic simulation and metabolome analysis of long-term erythrocyte storage in adenine-guanosine solution. PLoS One, 8(8), e71060.
O'Neill, D. P., & Robbins, P. A. (2017). A mechanistic physicochemical model of carbon dioxide transport in blood. Journal of Applied Physiology, 122(2), 283–295.
Occhipinti, R., & Boron, W. F. (2015). Mathematical modeling of acid-base physiology. Progress in Biophysics and Molecular Biology, 117(1), 43–58.
Occhipinti, R., & Boron, W. F. (2019). Role of carbonic anhydrases and inhibitors in acid-base physiology: Insights from mathematical modeling. International Journal of Molecular Sciences, 20(15), 3841.
Płoszczyca, K., Czuba, M., Chalimoniuk, M., Gajda, R., & Baranowski, M. (2021). Red blood cell 2,3-diphosphoglycerate decreases in response to a 30 km time trial under hypoxia in cyclists. Frontiers in Physiology, 12, 670977.
Rasmussen, J. K., & Boedtkjer, E. (2018). Carbonic anhydrase inhibitors modify intracellular pH transients and contractions of rat middle cerebral arteries during CO_2/HCO_3^- fluctuations. Journal of Cerebral Blood Flow and Metabolism, 38(3), 492–505.
Rees, S. E., Klaestrup, E., Handy, J., Andreassen, S., & Kristensen, S. R. (2010). Mathematical modelling of the acid-base chemistry and oxygenation of blood: A mass balance, mass action approach including plasma and red blood cells. European Journal of Applied Physiology, 108(3), 483–494.
Reithmeier, R. A., Casey, J. R., Kalli, A. C., Sansom, M. S., Alguel, Y., & Iwata, S. (2016). Band 3, the human red cell chloride/bicarbonate anion exchanger (AE1, SLC4A1), in a structural context. Biochimica et Biophysica Acta, 1858(7), 1507–1532.
Shartau, R. B., Baker, D. W., Crossley 2nd, D. A., & Brauner, C. J. (2016). Preferential intracellular pH regulation: Hypotheses and perspectives. The Journal of Experimental Biology, 219(15), 2235–2244.
Swietach, P., Tiffert, T., Mauritz, J. M., Seear, R., Esposito, A., Kaminski, C. F., Lew, V. L., & Vaughan-Jones, R. D. (2010). Hydrogen ion dynamics in human red blood cells. The Journal of Physiology, 588(24), 4995–5014.
Vilas, G., Krishnan, D., Loganathan, S. K., Malhotra, D., Liu, L., Beggs, M. R., Gena, P., Calamita, G., Jung, M., Zimmermann, R., Tamma, G., Casey, J. R., & Alexander, R. T. (2015). Increased water flux induced by an aquaporin-1/carbonic anhydrase II interaction. Molecular Biology of the Cell, 26(6), 1106–1118.
Zimna, A., Kaczmarska, M., Szczesny-Malysiak, E., Wajda, A., Bulat, K., Alcicek, F. C., Zygmunt, M., Sacha, T., & Marzec, K. M. (2021). An insight into the stages of ion leakage during red blood cell storage. International Journal of Molecular Sciences, 22(6), 2885.